SCIENTIFIC REPORTS

OPEN

SUBJECT AREAS:
ELECTRONIC DEVICES
GRAPHENE
METHODOLOGY
ELECTRONIC MATERIALS

Received
12 December 2012

Accepted
3 June 2013

Published
17 June 2013

Correspondence and requests for materials should be addressed to G.S. (gshi@tsinghua.edu.cn) or L.D. (Liming.Dai@case.edu)

Solution-processable graphene nanomeshes with controlled pore structures

Xiluan Wang[1], Liying Jiao[1], Kaixuan Sheng[1], Chun Li[1], Liming Dai[2] & Gaoquan Shi[1]

[1]Department of Chemistry, Tsinghua University, Beijing 100084, People's Republic of China, [2]Department of Macromolecular Science and Engineering, Case Western Reserve University, Cleveland, OH 44106, USA.

Graphene nanomeshes (GNMs) which can be cheaply produced on a large scale and processed through wet approaches are important materials for various applications, including catalysis, composites, sensors and energy related systems. Here, we report a method for large scale preparation of GNMs by refluxing reduced graphene oxide sheets in concentrated nitric acid solution (e.g., 8 moles per liter). The diameters of nanopores in GNM sheets can be readily modulated from several to hundreds nanometers by varying the time of acid treatment. The porous structure increased the specific surface areas of GNMs and the transmittances of GNM-based thin films. Furthermore, GNMs have large number of carboxyl groups at the edges of their nanopores, leading to good dispersibility in aqueous media and strong peroxidase-like catalytic activity.

Over the last several years, extensive work has been devoted to the syntheses and applications of graphene due to the excellent electrical, optical, mechanical and thermal properties associated with its unique atom-thick two-dimensional structure[1–7]. The most widely-used method to prepare graphene on a large scale at low cost is the reduction of graphene oxide (GO)[8–12]. However, the reduced graphene oxide (rGO) is insoluble, infusible and intractable[8–14]. The poor processability of neutral rGO precludes the possibility of using conventional material processing techniques to fabricate macroscopic rGO-based materials into desired shapes or structures. Furthermore, rGO sheets are normally composed of about 60% intact graphene islands of variable sizes interspersed with planar quasi-amorphous sp^2–bonded defect clusters, which predominantly incorporate a large number of carbon pentagons, heptagons, and hexagons[15]. The defect clusters of rGO sheets can be selectively removed to produce GNMs with more perfect graphene basal planes.

It is highly expected that the preparation of GNM to open the band gap of graphene[16,17] and increase its specific surface area (SSA) and transparency[18,19], resulting in the formation of a class of new fascinating materials for various applications in graphene-based composites, catalysis, sensors and energy related systems[20–22]. Up to now, high-quality single-layered GNMs have been prepared only by plasma or photocatalytic oxidation of graphene sheets using solid templates[16–18], while a bulk porous graphene material was obtained by chemical vapor deposition[23]. Unfortunately, only limited amounts of single-layered GNMs can be produced by these methods at high costs, and the resulting GNMs are not solution-processable, for example, by spin- or dip-coating, filtration and printing. Herein, we report a one-step solution method for the large scale production of GNMs by selectively removing the defect clusters of rGO sheets with nitric acid. This technique is readily scalable and conceptually different from those reported for preparing holey graphene sheets[16–23]. These GNM sheets have uniformly distributed nanopores, ranging from several to hundreds nanometers in diameters, and can be stably dispersed in aqueous media, including pure water.

Results

In a typical experiment, GNMs were prepared by refluxing rGO sheets in 8 mol L^{-1} nitric acid solution for 4, 6, 9 or 11 hours (see Supplementary Information for details). They are designated as GNM-n, where n refers to the time used for acid treatment (t_{at}). Similar technique has previously been used to purify single-walled carbon nanotubes (SWCNTs), removing the residual catalyst and amorphous carbons, at the expense of a significant destruction of SWCNTs[24]. In this study, we found that the defect clusters of rGO sheets can be selectively removed by the treatment with nitric acid to leave nanopores in the basal planes of rGO sheets due to the relatively higher chemical activeties intrinsically associated with the defect clusters. For instance, the GNM sheets prepared by

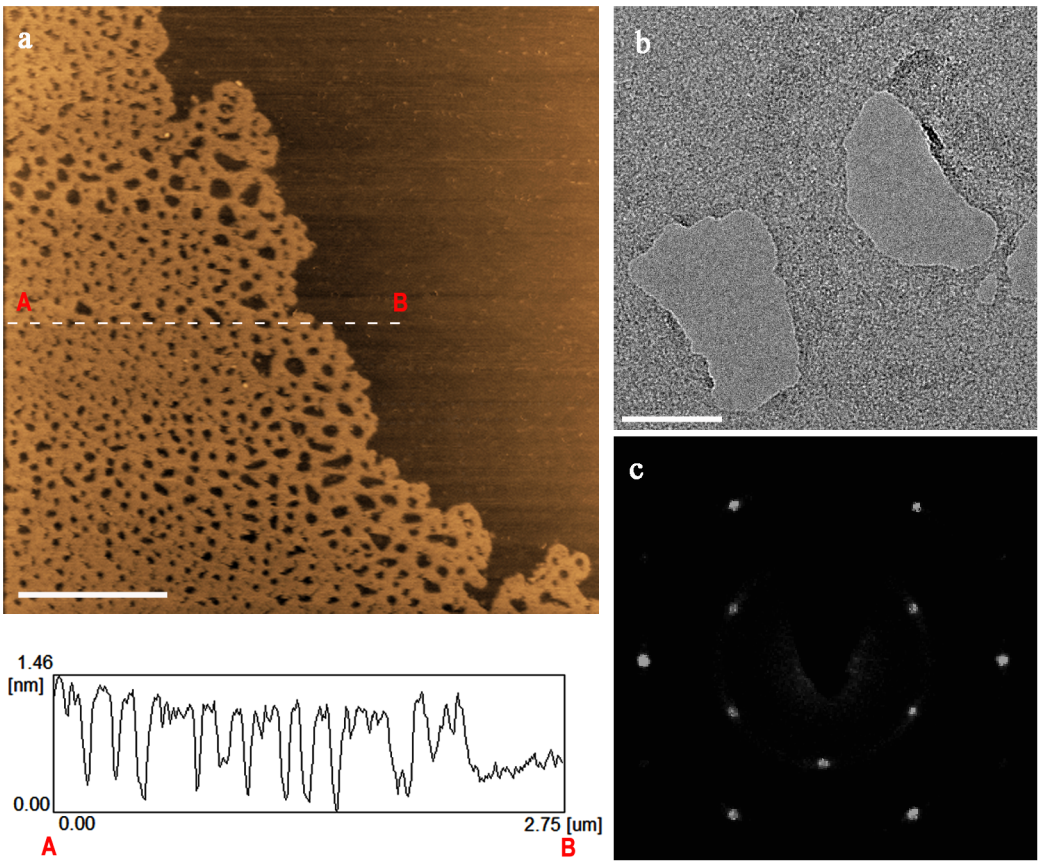

Figure 1 | Morphology and structure of a GNM-6 sheet. (a) Tapping mode AFM image of a GNM-6 sheet with a height frofile; scale bar = 1 μm. (b) A tyical HR-TEM image of a GNM-6 sheet; scale bar = 50 nm. (c) A SAED pattern of the basal plane surrounding the nanopores shown in (b).

treating rGO sheets with nitric acid for 6 h (GNM-6) show nanopores with diameters in the range of 0–90 nm (*ca.*90% of them ≤ 60 nm) and the pores are uniformly distributed over the whole GNM sheet (Figure 1a, Figure S1). The total area of nanopores within 1.00 μm^2 GNM-6 sheet was estimated to be about 0.46 μm^2. The lateral dimmensions of GNM-sheets are in the range of 3–5 μm, which are more uniform than those of rGO precusors (0.5–7 μm, Figure S2). The thickness of a GNM-6 sheet is around 1.0 nm according to the height profile of AFM image (Figure 1a), indicating a single-layer nature of rGO sheet[20]. High-resolution transmission electron microscope (HR-TEM) images of GNM-6 clearly demonstrate the nanoporous structure, as exemplified by Figure 1b showing a typical image of several nanopores. The nanopores with irregular shapes are surrounded by a graphene basal plane. The distances between neighbouring nanopores are typically in the range of several nanometers to about 50 nm. The selected area electron diffraction (SAED) pattern of the graphene basal plane shows a sharp hexgonal dffraction dots (Figure 1c), indicating a perfect crystalline structure with regular carbon framework. In comparison, the SAED pattern of a rGO sheet usually exhibits a halo ring arising from its defect clusters[25]. These results confirm that the defect clusters of rGO have been, at least, partially removed by the treatment with nitric acid.

Discussion

To reveal the mechanism for the nanopore formation in GNMs, we followed the morphological changes of GNMs with the time of nitric acid treatment. As shown in Figure 2, the number density of nanopores in GNMs decreased from 55 ± 6 μm^{-2} through 26 ± 2 to 15 ± 2 μm^{-2} with the t_{at} increased from 4 through 6 to 9 h. In the meantime, the total area of nanopores within 1.00 μm^2 of GNM sheet increased from 0.10 through 0.46 to 0.63 μm^2. At t_a = 11 h, the GNM sheets were broken up into tiny sheets. The pore sizes of GNMs also increased with the increase of t_{at} (Figure S1). For example, the pore diameters of GNM-4 are mainly in the range of 10 to 40 nm (>85%), while those of GNM-9 are mostly larger than 40 nm (>80%). Accordingly, the size and the number density of pores in GNM sheets can be regulated simply by varying t_{at}.

The selctive removal of the defect clusters in rGO sheets upon the acid treatment was further confirmed by X-ray photoelectron spectroscopy (XPS) and Raman measurements. As can be seen from Figure 3a, the acid-treatment-induced conversion of rGO to GNM reduced the intensities of the peak components associated with C-N, C-O (hydroxyl and epoxide) groups in the C 1s XPS spectra and enhanced the –C=O and –COOH peak intensities singinficantly[26]. The atomic contents of the carbon atoms related to –C=O and –COOH groups were caculated to be 4.63, 7.24, 7.51 and 8.26% for rGO, GNM-6, GNM-9 and GNM-11, respectively. These XPS results reflect that the defect clusters of rGO sheets were partially removed to form the nanopores with defective edges; because it has been previously reported that the C-N, hydroxyl and epoxide groups of rGO sheets are prodominately connected to the defect clusters on their basal planes while the –C=O and –COOH groups are mainly located at their edges[27,28].

The Raman spectrum for each of the GNMs shows a disorder-induced band (D-band) in the range 1300–1370 cm^{-1} and a first-order-allowed band (G-band) in the region of 1580–1600 cm^{-1} (Figure 3b)[25]. The intensity ratio of D/G bands for GNM-6, GNM-9 and GNM-11 were measured to be 0.93, 0.91 and 0.88, respectively. These values are much lower than the corresponding value for rGO (1.11), implying, once again, the removal of the quasi-amorphous sp^2-bonded carbons of rGO by the treatment with nitric acid. The

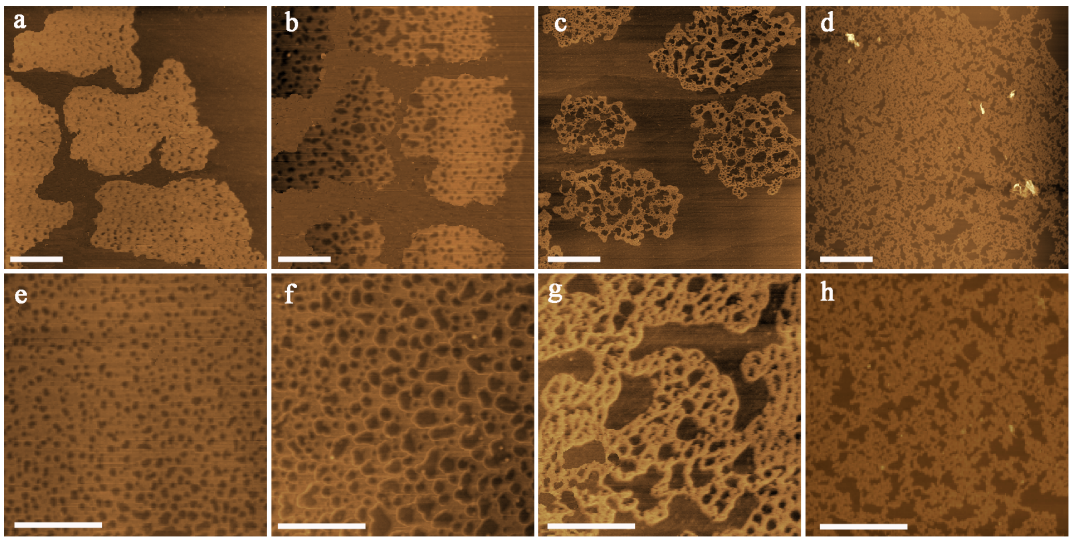

Figure 2 | The evolution of nanopores in GNMs. (a–h) AFM images of GNM-4 (a, e); GNM-6 (b, f), GNM-9 (c, g) and GNM-11 (d, h); (a–d) scale bar = 2 μm and (e–h) scale bar = 1 μm.

disorder carbons of GNMs are attributed to mainly those carbon atoms at the edges of the nanopores, as indicated by the XPS spectra (Figure 3a).

Owing to the presence of –C=O and –COOH groups at the nanopore edges, the GNMs can form stable dispersions in pure water (Figure 4a). The ionization of carboxy groups enhanced the repulsion force between graphene sheets to increase the solubilities of GNMs[25], as confirmed by Zeta potential measurements. It is known that a rGO dispersion is stable when its Zeta potential is <-30 mV[29]. In pure water (pH = 6.4), the Zeta potentials of GNM dispersions are in the range of -36 to -46 mV, and hence they are stable (Figure 4b). Indeed, a 2 mg mL^{-1} dispersion of GNM-6 in pure water did not show perticipation even after keeping at room temperature for over 1 week (Figure 4a). In contrast, rGO sheets cannot be stably dispersed in the same medium because of their relatively higher zeta potential (≈ -30 mV at pH = 6.4, Figure 4b).

To test the solution-processiblity of GNMs, we filtrated their stable aquesous dispersions (1 mg mL^{-1}) through porous polytetrafluoroethylene (PTFE) membranes to prepare GNM films (Figure S3). The X-ray diffraction pattern for each of the resultant GNM films shows a peak at $2\theta = 24.39^{\circ}$, which is higher than that of the corresponding peak for an rGO film ($2\theta = 23.22^{\circ}$) prepared under the same condition (Figure 4c). This result indicates that GNM sheets can be assembled into more compact "paper" with a d-space (3.65 Å) smaller than that of an rGO "paper" (3.83 Å)[25]. Furthermore, the full width at half-maximum (FWHM) values of the XRD peaks for GNM-6, GNM-9 and GNM-11 papers were measured to be 2.71°, 2.55° and 2.41°, respectively, all being much narrower than that of the rGO paper (4.20°). These results reveal that the graphene sheets in GNM papers have more ordered stacking structures than that in an rGO paper[20]. The cross-section SEM images of the films also indicate that the GNM-6 paper has a more compact stacking structure than that of the rGO paper (Figure S4). Therefore, the partial removal of oxgenated groups from the basal planes of rGO sheets decreased the d-spaces between graphene sheets, facilitating the formation of more ordered GNM films.

In view of the above mechanism and structural studies, we further tested the nanoporous structure of GNMs for optical transparency

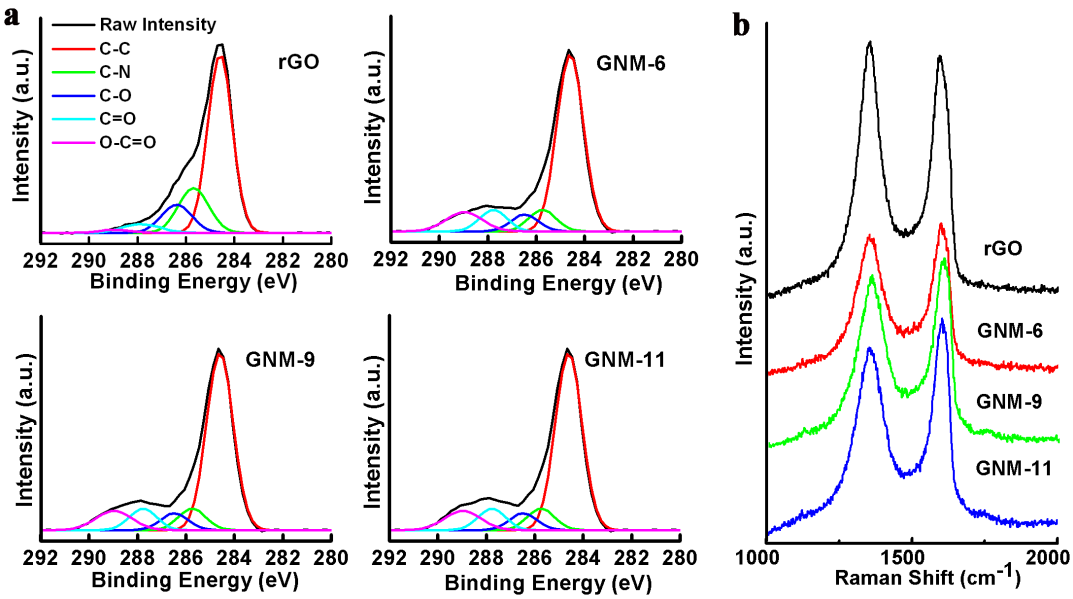

Figure 3 | Compositions and structures of GNMs. (a) C 1s XPS and (b) Raman spectra of rGO and GNMs.

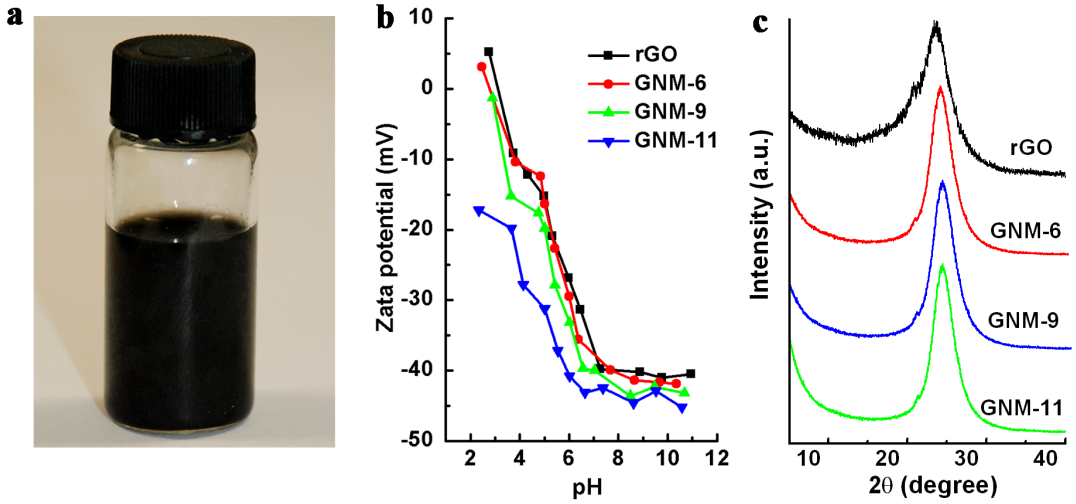

Figure 4 | Processability of GNMs and the structures of GNM papers. (a) A 2 mg mL^{-1} GNM-6 dispersion in pure water. (b) Zeta potentials of the aqueous dispersions of rGO and GNMs as a function of pH value. (c) XRD patterns of rGO and GNM films.

enhancement. The transmittances of thin GNM-6 films with different thicknesses deposited on poly(ethylene terephthalate) substrates are plotted in Figure 5a. As can be seen, the transmittance of a GNM-6 film is much higher than that of an rGO film at any given thickness investigated in the present work[30]. For example, a 21-nm thick GNM film has a transmittance of 85% at 550 nm (Figure 5a), but only 74% for its rGO counterpart. Due to its porous structure, the sheet resistance of a GNM-6 film is about one order of magnitude higher than that of a rGO film with the same thickness (Figure S5). However, thermal treatment of the GNM-6 film at 400°C in Ar for 3 h reduced its sheet resistance to a value comparable to that of the rGO film with negligible change in its transparency. More importantly, the nanoprous structure increased the specific surface area (SSAs) of GNMs significantly. The SSAs of GNM-4, GNM-6, GNM-9 and GNM-11 were measured by a standard methylene blue adsorption method to be 810 ± 46, 970 ± 60, 1010 ± 60 and 840 ± 35 m^2 g^{-1} (average of 3 samples), respectively. Thsese values are much larger than that of rGO (595 ± 75 m^2 g^{-1})[31].

The high content of –COOH groups and large SSAs of the GNMs make them promising for replacing intrinsic peroxidase catalysts for certain bioreactions or biosensors[32]. As a demonstration, we used GNM-6 or GNM-11 to catalyze the reaction of a peroxidase substrate, 3,3,5,5-tetramethyl benzidine (TMB), in the presence of H_2O_2 to produce a blue color reaction. The absorbance at 652 nm of the reaction system with a constant amount of catalyst is proportional to the reaction conversion or the catalytic activity of the catalyst (Figure 5b). Actually, the reaction conversion for the system with the GNM-6 (GNM-11) peroxidase catalyst is about 4.2 (5.0) times that of the widely-used horse horseradish peroxidase (HRP) and 2.1 (2.5) times that of GO after carrying out the reaction at room temperature for 12 h. This result reflects the unusuallly high catalytic activities of the newly-developed GNM peroxidase catalysts.

In conclusion, we have developed a cheap, convenient and effective chemical approach for large-scale synthesis of GNMs by refluxing rGO sheets in concentrated nitric acid, which can be readily scalable to industry levels. The porous structures of GNMs can be well controlled simply by regulating the reaction time. Due to its nanoporous nature, the resultant GNMs show high specific surface areas, improved optical transparencies and good solution-processability, making them attractive for various potential applications, including catalysis, energy storage, sensors and environmental protections.

Methods

GO was prepared by the oxidation of natural graphite powder (325 mesh) according to a modified Hummers' method (see Supplementary Information for details)[29,33,34]. rGO was synthesized by reducing the aqueous dispersion of GO with hydrazine hydrate according to the method reported in literature (see Supplementary Information for details)[29]. GNMs were prepared by mixing 50 mL rGO dispersion (0.1 mg mL^{-1}) with a certain amount of HNO_3 solution to form a mixture containing

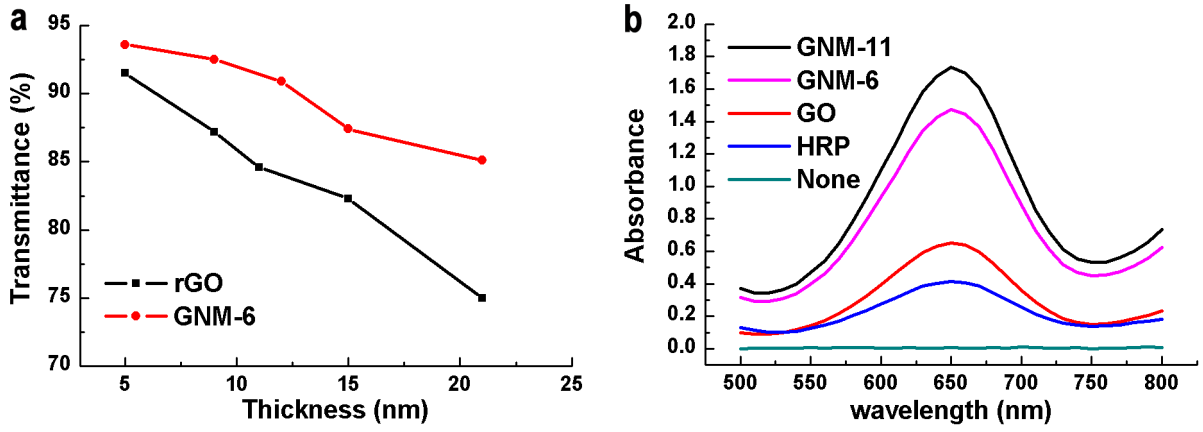

Figure 5 | Properties of GNMs. (a) Optical transmittance at 550 nm as a function of the film thickness. (b) UV-visible spectrum of the system containing 800 μmol L^{-1} TBM, 50 mmol L^{-1} H_2O_2 and 40 μg mL^{-1} HRP, GO, GNM-6 or GNM-11 after reaction at room temperature for 12 h.

8 mol L^{-1} HNO_3 and then refluxed at 100°C for 4, 6, 9 or 11 h (see Supplementary Information for details). The diluted suspension of rGO or GNM was subjected to vacuum filtration, leading to the deposition of an rGO or GNM film on the surface of a porous anodic aluminum oxide (AAO, pore size = 0.2 μm) membrane. Then the film was transferred to the surface of a poly(ethylene terephthalate) (PET) or quartz substrate and dried at 60°C. The annealing of GNM film was performed in a tube oven equipped with a quality vacuum system. The thickness of films was obtained by AFM measurement (see Supplementary Information for details).

The catalytic reactions were carried out by mixing 20 μg GO, GNM-6, GNM-11 or horseradish peroxidase (HRP) with 500 μL buffer solution (25 mmol L^{-1} NaH_2PO_4, pH 5.0, 35°C) containing 800 μmol L^{-1} 3,3,5,5-tetramethylbenzidine (TMB) and 50 mmol L^{-1} H_2O_2. Then, the UV-visible spectra of the reaction systems were recorded during the reaction processes.

The thicknesses of rGO and GNM sheets, and their films were measured by using a SPM 9600 atomic force microscope (Shimadzu) in tapping mode. The XRD patterns were recorded by using a D8 Advance X-Ray diffractometer with Cu-Kα radiation (λ = 1.5418 Å, Bruker, Germany). XPS measurements were performed on a PHI 550 EACA/SAM photoelectron spectrometer using Al Kα (1486.6 eV) radiation. Raman spectra were recorded on a RM 2000 Microscopic confocal Raman spectrometer (Renishaw PLC, England) using a 514 nm laser beam. The electrical conductivities of rGO or GNM films were measured using a four-probe conductivity test meter (KDY-1, Kunde Technology, Co., Ltd.) at room temperature. The transmittances of the rGO or GNM films at 550 nm and the UV-visible spectra of the catalytic reaction systems were measured by the use of a U-3010 UV-visible spectrometer (Hitachi, Japan). The zeta potentials of rGO and GNMs aqueous dispersions with various pH values were measured by the use of a zeta sizer nanosystem (Malvern Instruments). The HR-TEM image of a typical nanopore of GNMs was examined by using an annular-dark-field scanning transmission electron microscope (ADF-STEM) (FEI Tecnai F20 field emission gun, 200 kV, with Fischione annular-dark-field detector). Selected area electron diffraction (SAED) patterns were also recorded on the same instrument.

1. Novoselov, K. S. *et al.* Electric field effect in atomically thin carbon films. *Science* **306**, 666–669 (2004).
2. Nair, R. R. *et al.* Fine structure constant defines visual transparency of graphene. *Science* **320**, 1308 (2008).
3. Tombros, N., Jozsa, C., Popinciuc, M., Jonkman, H. T. & van Wees, B. J. Electronic spin transport and spin precession in single graphene layers at room temperature. *Nature* **448**, 571–574 (2007).
4. Li, X., Wang, X., Zhang, L., Lee, S. & Dai, H. Chemically Derived, Ultrasmooth Graphene Nanoribbon Semiconductors. *Science* **319**, 1229–1232 (2008).
5. Li, X. *et al.* Large-area synthesis of high-quality and uniform graphene films on copper foils. *Science* **324**, 1312–1314 (2009).
6. Zhu, Y. *et al.* Carbon-based supercapacitors produced by activation of graphene. *Science* **332**, 1537–1541 (2011).
7. Chen, Z. P. *et al.* Three-dimensional flexible and conductive interconnected graphene networks grown by chemical vapour deposition. *Nat. Mater.* **10**, 424–428 (2011).
8. Loh, K. P., Bao, Q. L., Ang, P. K. & Yang, J. X. The chemistry of graphene. *J. Mater. Chem.* **20**, 2277–2289 (2010).
9. Stankovich, S., Piner, R. D., Nguyen, S. T. & Ruoff, R. S. Synthesis and exfoliation of isocyanate-treated graphene oxide nanoplatelets. *Carbon* **44**, 3342–3347 (2006).
10. Stankovich, S. *et al.* Graphene-based composite materials. *Nature* **442**, 282–286 (2006).
11. Moon, I. K., Lee, J., Ruoff, R. S. & Lee, H. Reduced graphene oxide by chemical graphitization. *Nat. Commun.* **1**, 73; DOI: 10.1038/ncomms1067 (2010).
12. Xu, Z. & Gao, C. Graphene chiral liquid crystals and macroscopic assembled fibres. *Nat. Commun.* **2**, 571; DOI: 10.1038/ncomms1583 (2011).
13. Xu, Y., Bai, H., Lu, G., Li, C. & Shi, G. Flexible graphene films via the filtration of water-soluble noncovalent functionalized graphene sheets. *J. Am. Chem. Soc.* **130**, 5856–5857 (2008).
14. Bai, H., Li, C. & Shi, G. Functional composite materials based on chemically converted graphene. *Adv. Mater.* **23**, 1089–1115 (2011).
15. Gómez-Navarro, C. *et al.* Atomic structure of reduced graphene oxide. *Nano Lett.* **10**, 1144–1148 (2010).
16. Bai, J., Zhong, X., Jiang, S., Huang, Y. & Duan, X. Graphene nanomesh. *Nat. Nanotechnol.* **5**, 190–194 (2010).
17. Zeng, Z. *et al.* Fabrication of Graphene Nanomesh by Using an Anodic Aluminum Oxide Membrane as a Template. *Adv. Mater.* **24**, 4138–4142 (2012).
18. Akhavan, O. Graphene nanomesh by ZnO nanorod photocatalysts. *ACS Nano* **4**, 4174–4180 (2010).
19. Roth, S. & Park, H. J. Nanocarbonic transparent conductive films. *Chem. Soc. Rev.* **39**, 2477–2483 (2010).
20. Han, T. H., Huang, Y. K., Tan, A. T., Dravid, V. P. & Huang, J. Steam etched porous graphene oxide network for chemical sensing. *J. Am. Chem. Soc.* **133**, 15264–15267 (2011).
21. Zhao, X., Hayner, C. M., Kung, M. C. & Kung, H. H. Flexible holey graphene paper electrodes with enhanced rate capability for energy storage applications. *ACS Nano* **5**, 8739–8749 (2011).
22. Ning, G. *et al.* Gram-scale synthesis of nanomesh graphene with high surface area and its application in supercapacitor electrodes. *Chem. Commun.* **47**, 5976–5978 (2011).
23. Ning, G. *et al.* Chemical vapor deposition derived flexible graphene paper and its application as high performance anodes for lithium rechargeable batteries. *J. Mater. Chem.* **A 1**, 408–414 (2013).
24. Hu, H., Zhao, B., Itkis, M. E. & Haddon, R. C. Nitric acid purification of single-walled carbon nanotubes. *J. Phys. Chem. B.* **107**, 13838–13842 (2003).
25. Xu, Y., Sheng, K., Li, C. & Shi, G. Highly conductive chemically converted graphene prepared from mildly oxidized graphene oxide. *J. Mater. Chem.* **21**, 7376–7380 (2011).
26. Stankovich, S. *et al.* Synthesis of graphene-based nanosheets via chemical reduction of exfoliated graphite oxide. *Carbon* **45**, 1558–1565 (2007).
27. Gao, W., Alemany, L. B., Ci, L. & Ajayan, P. M. New insights into the structure and reduction of graphite oxide. *Nat. Chem.* **1**, 403–408 (2009).
28. Dreyer, D. R., Park, S., Bielawski, C. W. & Ruoff, R. S. The chemistry of graphene oxide. *Chem. Soc. Rev.* **39**, 228–240 (2010).
29. Li, D., Muller, M. B., Gilje, S., Kaner, R. B. & Wallace, G. G. Processable aqueous dispersions of graphene nanosheets. *Nat. Nanotechnol.* **3**, 101–105 (2008).
30. Becerril, H. A. *et al.* Evaluation of solution-processed reduced graphene oxide films as transparent conductors. *ACS Nano* **2**, 463–470 (2008).
31. Santamarina, J. C., Klein, K. A., Wang, Y. H. & Prencke, E. Specific surface: determination and relevance. *Can. Geotech. J.* **39**, 233–241 (2002).
32. Song, Y., Qu, K., Zhao, C., Ren, J. & Qu, X. Graphene oxide: intrinsic peroxidase catalytic activity and its application to glucose detection. *Adv. Mater.* **22**, 2206–2210 (2010).
33. Sheng, K., Sun, Y., Li, C., Yuan, W. & Shi, G. Ultrahigh-rate supercapacitors based on eletrochemically reduced graphene oxide for ac line-filtering. *Sci. Rep.* **2**, 247; DOI:10.1038/srep00247 (2012).
34. Hummers, W. S. & Offeman, R. E. Preparation of graphitic oxide. *J. Am. Chem. Soc.* **80**, 1339–1339 (1958).

Acknowledgements

This work was supported by national basic research program of China (973 Program, 2012CB933402), natural science foundation of china (91027028, 50873092), and NSFC-NSF (DMR-1106160). The authors thank Prof. Linjie Zhi and Mr Yuying Jia at National Center of Nanoscience and Nanotechnology of China for assistance with TEM experiments.

Author contributions

G.S. and L.D. conceived and designed the experiments. X.W. performed the experiments and analysed the data. L.J., K.S. and C.L. provided helps in the experiments. X.W., G.S., L.D. and C.L. co-wrote the manuscript. All authors discussed the results and commented on the manuscript.

Additional information

Supplementary information accompanies this paper at http://www.nature.com/scientificreports

Competing financial interests: The authors declare no competing financial interests.

How to cite this article: Wang, X. *et al.* Solution-processable graphene nanomeshes with controlled pore structures. *Sci. Rep.* **3**, 1996; DOI:10.1038/srep01996 (2013).